

Effective collision strengths for excitation and de-excitation of nebular [O III] optical and infrared lines with κ distributed electron energies

P.J. Storey¹, Taha Sochi^{1*}

¹*Department of Physics and Astronomy, University College London, Gower Street, London WC1E 6BT, UK*

Accepted 2015 March 3. Received 2015 February 14; in original form 2015 January 15

ABSTRACT

We present effective collision strengths for electron excitation and de-excitation of the ten forbidden transitions between the five lowest energy levels of the astronomically abundant doubly-ionised oxygen ion, O^{2+} . The raw collision strength data were obtained from an R-matrix intermediate coupling calculation using the Breit-Pauli relativistic approximation published previously by the authors. The effective collision strengths were calculated with κ -distributed electron energies and are tabulated as a function of the electron temperature and κ .

Key words: atomic data – atomic processes – radiation mechanisms: non-thermal – planetary nebulae: general – infrared: general.

1 INTRODUCTION

The spectral lines of doubly-ionised oxygen, O^{2+} , are important diagnostic tools in a variety of astronomical and astrophysical situations, such as solar and nebular studies, due to the abundance of this ion in these environments and the brightness of a number of its lines (Aggarwal & Keenan 1999). They are used for instance to determine the oxygen abundance and other physical conditions in the Milky Way and other galaxies out to substantial cosmological distances (Maiolino *et al* 2008). There has been a recent advocacy (Nicholls *et al* 2012, 2013) of the use of non Maxwell-Boltzmann (MB) electron energy distributions in the analysis of the spectra of planetary nebulae (PNe) and H II regions. It has been proposed that the discrepancy between the results for elemental abundance and electron temperature obtained from the optical recombination lines (ORLs) and those obtained from the collisionally-excited lines (CELs) could be resolved if the free electron energies are described by a κ -distribution (Vasyliunas 1968) rather than a MB one. Storey & Sochi (2013) attempted to test this hypothesis using a subset of dielectronic recombination lines to directly sample the free electron energy distribution. No evidence was found for departures from a MB distribution in a small sample of PNe but the uncertainties in the observational data made it impossible to rule out such departures. Zhang *et al* (2014) modelled the shape of the Balmer continuum in the spectra of a sample of PNe and concluded that both a model comprising two MB distributions of different tem-

peratures or κ -distributions matched the spectra within the observational errors. However, Storey & Sochi (2014) carried out the same modelling on the extreme PN, Hf 2-2, and concluded that the probability that the spectrum corresponds to a κ -distribution is extremely low.

The present paper is part of a series of papers by the authors intended to make possible a spectroscopic investigation of whether a κ electron energy distribution can provide a consistent explanation of the spectra of the thin and relatively cold plasma found in planetary nebulae and H II regions. The [O III] lines are very strong in all PNe and the corresponding recombination lines of O II have also been recorded in many nebulae exhibiting varying degrees of disagreement between ORL and CEL abundances and temperatures. Indeed, the abundances derived from the [O III] forbidden lines and from the O II recombination lines are one of the primary sources for the ORL/CEL discrepancy. We therefore aim to provide in this series of papers κ -dependent recombination coefficients for H I and O II and κ -dependent collision strengths for the electron excitation and de-excitation of the [O III] lines. With these theoretical data we aim to answer the question whether any single κ -distribution can explain the relative intensities of the [O III] forbidden lines and corresponding O II recombination lines in a range of PNe and, if so, what is the resulting O^{2+}/H abundance ratio.

In Storey *et al* (2014) the available theoretical parameters for electron collisional excitation of the [O III] forbidden lines were investigated and new collision strength data for the ten transitions between the five lowest levels of the ground configuration were generated using a Breit-Pauli rel-

* E-mail: t.sochi@ucl.ac.uk

ativistic model. In Storey & Sochi (2015) the κ -distributed hydrogen recombination data were provided. The purpose of the present paper is to investigate κ -distributed effective collision strengths of the [O III] forbidden transitions. What remains is the O II recombination with a κ electron distribution which will be the subject of a forthcoming paper.

2 COLLISION STRENGTHS

There are a considerable number of studies dealing with the collision strengths of O^{2+} and their thermally-averaged values (e.g. Baluja *et al* (1980); Aggarwal (1983, 1985, 1993); Lennon & Burke (1994); Aggarwal & Keenan (1999); Palay *et al* (2012); Storey *et al* (2014); Mendoza & Bautista (2014)). However, most of the past studies provided a limited amount of effective collision strength data; moreover, except the last one, the provided data are based on a Maxwell-Boltzmann electron energy distribution. Storey *et al* (2014) reviewed the existing theoretical work and concluded that there is good agreement between their new collision strength results and all the past high-quality calculations. However, they found significant differences with the work of Palay *et al* (2012) which, they argued, were probably due to the small number of target states used by those authors, omitting key terms of the $2p^4$ electron configuration. The most recent work of Mendoza & Bautista (2014) also uses a limited number of target states which omits the $2p^4$ terms and the calculations were made with an implementation of the Intermediate Coupling Frame Transformation (ICFT) method of Griffin, Badnell & Pindzola (1998) which is potentially problematic for the deeply closed channels that are encountered in low energy scattering from O^{2+} (Storey *et al* 2014). Recently, Aggarwal & Keenan (2015) have suggested that the Be-sequence ICFT calculations of Fernández-Mencheró *et al* (2014) might be unreliable due to their use of the ICFT method, quoting Storey *et al* (2014) as evidence of potential problems. It is important to emphasise that the problems encountered in the ICFT calculations for $O^{2+} + e^-$ scattering were due to a specific combination of circumstances and cannot be assumed to have occurred for any previous ICFT work. In the ICFT approach, closed channel wavefunctions are integrated inwards to the boundary of the R-matrix inner region. The target orbitals in the $O^{2+} + e^-$ calculation of Storey *et al* (2014) were very compact, comprising only $n = 2$ spectroscopic orbitals and short range $n = 3$ and 4 correlation orbitals. For low charge ions, deeply closed channels with small effective quantum number can arise and for $O^{2+} + e^-$ the inward integration of these deeply closed channels to small values of radius developed significant exponentially growing terms which distorted the results.

In Figure 1 we compare the MB-averaged collision strengths for the ${}^3P_0 - {}^1S_0$ transition from Lennon & Burke (1994), Aggarwal & Keenan (1999), Palay *et al* (2012) and Mendoza & Bautista (2014) with those of Storey *et al* (2014) as a function of electron temperature. As in Storey *et al* (2014) we show the percentage difference from the Storey *et al* (2014) results in each case. The values plotted for Mendoza & Bautista (2014) were calculated by us from their collision strength data as privately supplied to us. As with the Palay *et al* (2012) results, the Mendoza & Bautista (2014) values differ significantly from those of Storey *et al* (2014)

and previous large scale calculations. A possible source of the difference between the results of Storey *et al* (2014) and Mendoza & Bautista (2014) is that the latter's collision strengths extend to a higher energy than the former's. However, on truncating the energy range of the Mendoza & Bautista (2014) collision strengths to the same range used by Storey *et al* (2014) we found that the effective collision strengths are only marginally different in the temperature range 100–20000 K. We therefore continue to maintain the view expressed by Storey *et al* (2014) that there is no reason to believe that the consensus of the results of Lennon & Burke (1994), Aggarwal & Keenan (1999) and Storey *et al* (2014), which all agree within 10%, is in error. A similar pattern is seen in the other forbidden transitions among the lowest five levels.

3 THEORETICAL BACKGROUND

The electron impact collision strength, Ω , is a dimensionless quantity used to quantify the intrinsic probability of collisional excitation and de-excitation in an atomic transition at a particular electron energy. The effective collision strength is defined as the collision strength averaged with respect to an electron energy distribution function, and hence it is obtained by convolving the collision strength with a distribution function. The effective collision strength of electron excitation, Υ , from a lower state i to an upper state j is defined by

$$\Upsilon_{i \rightarrow j} = \frac{\sqrt{\pi}}{2} e^{\left(\frac{\Delta E_{ij}}{k_B T}\right)} \int_0^\infty \Omega_{ij}(\epsilon_i) \sqrt{\frac{k_B T}{\epsilon_i}} f(\epsilon_i) d\epsilon_j \quad (1)$$

where T is the effective temperature, k_B is the Boltzmann constant, ϵ_i and ϵ_j are the free electron energy relative to the states i and j respectively, $\Delta E_{ij} (= \epsilon_i - \epsilon_j)$ is the energy difference between the two atomic states, $\Omega_{ij}(\epsilon_i)$ is the collision strength of the transition between the i and j states, and $f(\epsilon_i)$ is the electron energy distribution function. Similarly, the effective collision strength of electron de-excitation, \mathcal{J} , from an upper state j to a lower state i of a species is given by

$$\mathcal{J}_{j \rightarrow i} = \frac{\sqrt{\pi}}{2} \int_0^\infty \Omega_{ij}(\epsilon_j) \left(\frac{k_B T}{\epsilon_j}\right)^{1/2} f(\epsilon_j) d\epsilon_j \quad (2)$$

The electron distribution function is usually assumed a Maxwell-Boltzmann which is given by

$$f_{\text{MB}}(\epsilon, T) = \frac{2\sqrt{\epsilon}}{\sqrt{\pi} (k_B T)^3} e^{-\frac{\epsilon}{k_B T}} \quad (3)$$

based on a thermodynamic equilibrium state. Similar thermal-averaging procedures with respect to other electron distribution functions can also apply to reflect non-equilibrium states. The most widely used non-equilibrium distribution function is the κ distribution which is given, in one of its common forms, by (Vasyliunas 1968; Summers & Thorne 1991)

$$f(\epsilon, T, \kappa) = \frac{2\sqrt{\epsilon} \Gamma(\kappa + 1)}{\sqrt{\pi} (k_B T)^3 (\kappa - \frac{3}{2})^3 \Gamma(\kappa - \frac{1}{2}) \left(1 + \frac{\epsilon}{(\kappa - \frac{3}{2}) k_B T}\right)^{\kappa+1}} \quad (4)$$

where κ is a parameter characterising the distribution and takes values in the interval $(\frac{3}{2}, \infty)$, and Γ is the gamma function of the given arguments.

It should be remarked that Υ and \mathcal{J} are identical, by definition, for the Maxwell-Boltzmann distribution but are generally different for other types of electron distribution function such as the κ distribution. Also, the κ distribution converges to the Maxwell-Boltzmann distribution for large values of κ although in many cases the convergence practically occurs at moderate values of κ .

4 EFFECTIVE COLLISION STRENGTHS

We use the previously published raw collision strength data of Storey *et al* (2014). These were generated using a 72-term atomic target with the Breit-Pauli Hamiltonian terms in the intermediate coupling approximation as implemented in the UCL-Belfast-Strathclyde R-matrix code¹ (Berrington *et al* 1995). The limits of the effective collision strength data are the same as the limits of the original raw collision strength data that is: the data are related only to the ten transitions between the five lowest levels of the ion and a free electron excitation energy up to about 1.3 Rydberg. This provides effective collision strengths with a temperature up to 25000 K. These limits were adopted mainly for the relevance of the data to thin and relatively cold plasma found in planetary nebulae and H II regions. Mendoza & Bautista (2014) have presented some graphical comparisons of collision strengths averaged over κ -distributions for some [O III] transitions but very limited numerical results and only for MB distributions. Our data are therefore the first comprehensive set of its kind in the public domain as far as we know.

The data set accompanying this paper² consists of ten Υ files and ten \mathcal{J} files where each file is dedicated to one of the ten possible transitions between the five lowest levels of O²⁺ as given in Table 1. In this regard we define a scaled Upsilon quantity, Υ_s , by

$$\Upsilon_s = \Upsilon e^{\frac{-\Delta E_{ij}}{k_B T}}, \quad (5)$$

to compensate for the large values of Υ when T is low and ΔE_{ij} is large. We also impose a cut-off limit for the acceptance of the scaled Upsilon values; the essence of this condition is that any value that falls below 10^{-4} of the corresponding value at $T = 10^4$ K for the given κ should be dropped. We use the indicator “99999999” to mark these dropped entries for the purpose of keeping the rectangular structure of these tables. The physical basis for imposing the cut-off condition is that since the scaled Upsilon is proportional to the excitation rate coefficient, apart from a $T^{-1/2}$ factor, there is no practical use of the excitation rate if it is very small compared to the generally-accepted standard thermal condition in photoionised nebulae which is an MB distribution at $T = 10^4$ K.

The collisional excitation rate coefficients, q_{ij} , can be

obtained from the scaled Upsilon, Υ_s , using the following formula

$$q_{ij} = \frac{2\sqrt{\pi}c\alpha a_0^2}{\omega_i} \sqrt{\frac{R}{k_B T}} \Upsilon_s \simeq \frac{8.629 \times 10^{-6} \Upsilon_s}{\omega_i \sqrt{T}}, \quad (\text{cgs units}) \quad (6)$$

where ω_i is the statistical weight of state i , c is the speed of light in vacuum, α is the fine structure constant, a_0 is the Bohr radius, and R is the Rydberg energy constant and where the temperature is in Kelvin. Similarly, the collisional de-excitation rate coefficients, q_{ji} , can be obtained from the Downsilons, \mathcal{J} , using the following formula

$$q_{ji} = \frac{2\sqrt{\pi}c\alpha a_0^2}{\omega_j} \sqrt{\frac{R}{k_B T}} \mathcal{J} \simeq \frac{8.629 \times 10^{-6} \mathcal{J}}{\omega_j \sqrt{T}} \quad (\text{cgs units}) \quad (7)$$

where ω_j is the statistical weight of state j .

In each one of the aforementioned files, the 10-based logarithm of the effective collision strengths, Υ_s and \mathcal{J} , are tabulated in a rectangular array where the columns represent 10-based logarithmic electron temperatures [$\log_{10} T = 2.0(0.025)4.3$] while the rows represent κ which ranges between $1.6 - 10^6$ in unevenly-spaced periods [1.600(0.025)1.975, 2.0(0.1)2.9, 3.0(0.2)4.8, 5.0(0.5)9.5, 10(1)19, 20(2.5)47.5, 50(5)95, 100(25)175, 200(50)450, 500(100)900, 1000(1000)5000, 10000, 50000, 100000 and 1000000]. The T and κ grids are constructed to satisfy the condition that the maximum percentage error in Υ_s or \mathcal{J} from linear interpolation as a function of T or κ , between any two consecutive \log_{10} values in the data files, should not exceed 1% at the mid-point. More details about the interpolation errors for these tables are given in Table 2. The structure and contents of the data files are fully explained in the README file that associates the data set. A sample of these data for the 1-5 transition are presented in Table 3 for the logarithmic scaled Upsilon and in Table 4 for the logarithmic Downsilon.

In Figure 2 we show contour plots of Υ_s/\sqrt{T} as a function of T and $1/\kappa$ for three representative transitions. In this and subsequent contour plots the values are base 10 logarithms of the relevant quantity, normalised to the value for an MB distribution at 10^4 K, which we will refer to as the “standard PN conditions”. The plotted quantity is proportional to the excitation rate coefficient for each transition. The 1-4 transition is one of the means of exciting level 4, the ¹D₂ level, which gives rise to the important $\lambda\lambda 4959, 5007$ lines. The plot for this transition shows that the 1-4 excitation rate coefficient at 10^4 K is largely insensitive to the value of κ for values of κ larger than about 3. The picture is different for the 1-5 transition which excites the $\lambda 4363$ line which, by comparison with the $\lambda\lambda 4959, 5007$ lines is a temperature diagnostic. The contour plot for this transition shows that the excitation rate coefficient is sensitive to κ in such a way that the standard PN value can occur at lower temperatures as κ decreases. Hence we can expect that the ratio of the intensities of the lines from level 4 and 5, which are commonly used as a temperature diagnostic, will also be sensitive to the value of κ .

In Figure 3 we show a contour plot of the principal [O III] temperature diagnostic, the ratio of the sum of the emission coefficients, ϵ , of the two lines $\lambda\lambda 4959, 5007$ to the $\lambda 4363$ line at an electron number density of 10^4 cm^{-3} . The emission coefficients were computed using a model atom

¹ See Badnell: R-matrix write-up on WWW. URL: amdpp.phys.strath.ac.uk/tamoc/codes/serial/WRITEUP.

² The complete data generated in this work can be obtained in electronic format with full precision from the Centre de Données astronomiques de Strasbourg (CDS) database.

Table 1. The five lowest energy levels of O^{2+} with their experimental energies, E_{ex} , in wavenumbers (cm^{-1}). These values were obtained from the National Institute of Standards and Technology database (www.nist.gov).

Index	Level	E_{ex}
1	$1s^2 2s^2 2p^2 \ ^3P_0$	0.00
2	$1s^2 2s^2 2p^2 \ ^3P_1$	113.18
3	$1s^2 2s^2 2p^2 \ ^3P_2$	306.17
4	$1s^2 2s^2 2p^2 \ ^1D_2$	20273.27
5	$1s^2 2s^2 2p^2 \ ^1S_0$	43185.74

comprising the five energetically lowest levels, and only electron collisional excitation and de-excitation and spontaneous radiative transitions were included. The radiative transition probabilities were taken from Storey & Zeippen (2000), which we prefer to the more recent calculations of Fischer & Tachiev (2004) for O^{2+} since the former calculation incorporates relativistic corrections to the magnetic dipole operator. Adding these corrections yields a more accurate value for the well observed $\lambda 4959$, $\lambda 5007$ branching ratio which was in disagreement with theory until the work of Storey & Zeippen (2000). The plot shows that the loci of the values of temperature and κ where the MB value is reproduced always lies at lower temperatures as κ decreases and the distribution moves away from MB. For example, the predicted “standard” value for the line ratio of 194 is also obtained at $T \approx 6300$ K when $\kappa = 10$. The predicted line intensities are much lower at 6300 K than at the standard temperature of 10^4 K, so the number density of O^{2+} ions implied by a given measured line flux is larger.

In Figure 4 we show a contour plot of the O^{2+} number density, assuming a fixed intensity for the $\lambda 5007$ line, as a function of temperature and κ . For the example above, we find that at $T \approx 6300$ K and $\kappa = 10$ the number density is 3.2 times larger than that derived for standard conditions. The general conclusion therefore is that the observed optical [O III] line ratios can be modelled using a non-MB κ -distribution but with lower temperature and higher derived O^{2+} number density.

5 CONCLUSIONS

In the present paper, the effective collision strengths for electron excitation and de-excitation between the lowest five levels of O^{2+} are computed with a κ electron energy distribution using a previously published set of collision strengths. Extensive tabulations of the effective collision strengths as a function of temperature and κ are provided. We also illustrate and discuss the general behaviour of the most commonly used [O III] visible lines as a function of these two variables, and the effect on abundance determinations of adopting non-Maxwellian distributions for the free electrons. This work is intended to provide the data required for modelling and analysing optically thin plasma found mainly in planetary nebulae and H II regions, where it has been suggested that a non-MB κ electron distribution may apply and could provide a solution to the long standing problem in nebular physics of the contradiction between the results of elemen-

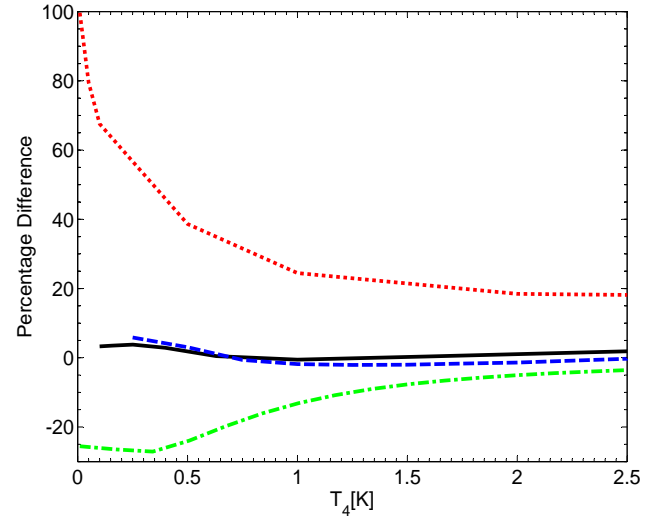


Figure 1. Percentage difference of thermally averaged collision strengths from our 72-term Breit-Pauli calculation versus temperature in 10^4 K for the transition 1-5. Results are from Lennon & Burke (1994) (solid black line), Aggarwal & Keenan (1999) (dashed blue line), Palay *et al* (2012) (dotted red line), and Mendoza & Bautista (2014) (dash-dotted green line).

tal abundance and electron temperature as obtained from optical recombination lines versus those obtained from collisionally excited lines.

6 ACKNOWLEDGMENT

The work of PJS was supported in part by STFC (grant ST/J000892/1). The authors would like to thank C. Mendoza and M.A. Bautista for sharing their data and atomic model.

REFERENCES

- Aggarwal K.M., 1983, ApJS, 52, 387
- Aggarwal K.M., 1985, A&A, 146, 149
- Aggarwal K.M., 1993, ApJS, 85, 197
- Aggarwal K.M., Keenan F.P., 1999, ApJS, 123, 311
- Aggarwal K.M., Keenan F.P., 2015, arXiv:1501.00808
- Baluja K.L., Burke P.G., Kingston A.E., 1980, J. Phys. B, 13, 829
- Berrington K.A., Eissner W.B., Norrington P.H., 1995, Comp. Phys. Comm., 92, 290
- Fernández-Mencheró L., Del Zanna G., Badnell N.R., 2014, A&A, 566, A104
- Fischer C.F., Tachiev G., 2004, At. Data. Nucl. Data Tables, 87, 1
- Griffin D.C., Badnell N.R., Pindzola M.S., 1998, J. Phys. B, 31, 3713
- Lennon D.J., Burke V.M., 1994, A&AS, 103, 273
- Maiolino R., Nagao T., Grazian A., *et al*, 2008, A&A, 488, 463
- Mendoza C., Bautista M.A., 2014, ApJ, 785, 91
- Nicholls D.C., Dopita M.A., Sutherland R.S., 2012, ApJ, 752, 148

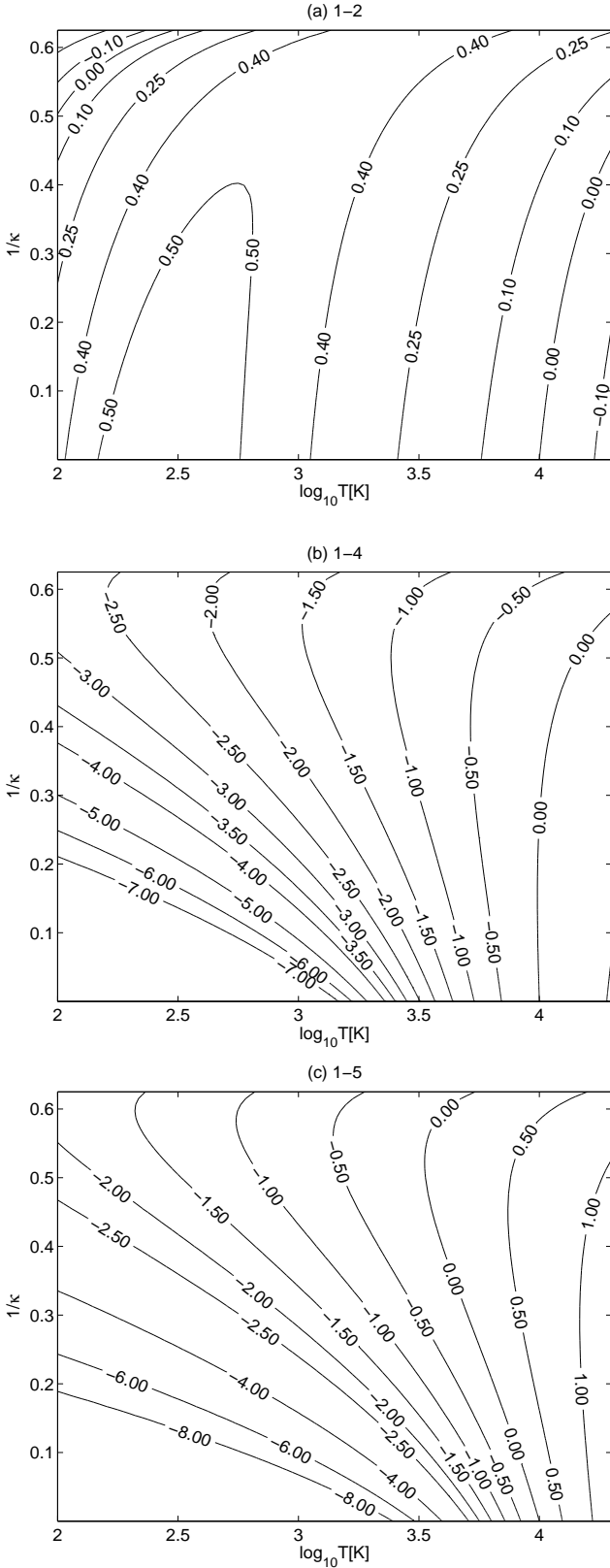


Figure 2. Contour plots for the \log_{10} scaled Upsilon (Equation 5) for the transitions (a) 1-2, (b) 1-4 and (c) 1-5 as functions of $\log_{10}T$ in K and $1/\kappa$. The scaled Upsilon values were first normalised to the square root of their temperature (\sqrt{T}) then to a reference value of Upsilon of a MB distribution at $T = 10^4$ K.

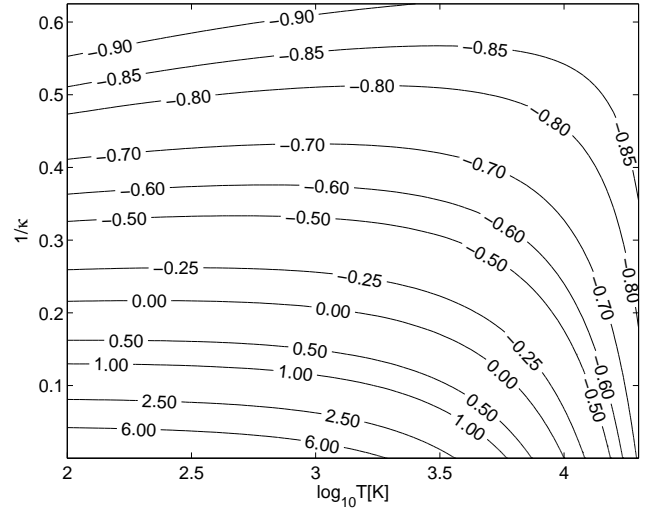


Figure 3. A contour plot of $\log_{10}[(\epsilon(\lambda 4959) + \epsilon(\lambda 5007))/\epsilon(\lambda 4363)]$ as a function of $\log_{10}T$ in K and $1/\kappa$, normalised to the MB value at $T = 10^4$ K.

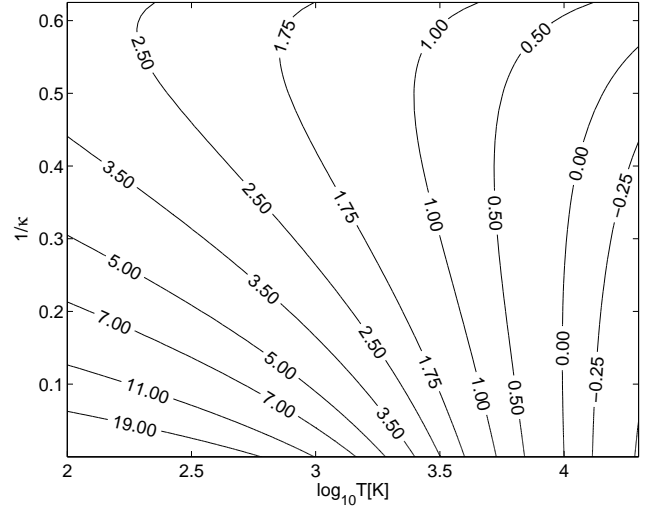


Figure 4. A contour plot of the \log_{10} of the O^{2+} number density derived from $\lambda 5007$ line as a function of $\log_{10}T$ in K and $1/\kappa$, normalised to the value derived from an MB distribution at $T = 10^4$ K.

- Nicholls D.C., Dopita M.A., Sutherland R.S., Kewley L.J., Palay E., 2013, ApJS, 207, 1
 Palay E., Nahar S.N., Pradhan A.K., Eissner W., 2012, MNRAS Let., 423, L35
 Storey P.J., Sochi T., 2013, MNRAS, 430, 599
 Storey P.J., Sochi T., 2014, MNRAS, 440, 2581
 Storey P.J., Sochi T., Badnell N.R., 2014, MNRAS, 441, 3028
 Storey P.J., Sochi T., 2015, MNRAS, 446, 1864
 Storey P.J., Zeppen, C., 2000, MNRAS, 312, 813
 Summers D., Thorne R.M. 1991, Phys. Fluids B, 3, 1835
 Vasyliunas V.M., 1968, JGR, 73, 2839
 Zhang Y., Liu X-W., Zhang B., 2014, ApJ, 780, 93

Table 2. Maximum and average error in interpolating the logarithmic values of scaled Upsilon and Downsilon in T and κ where MET=maximum absolute percentage error in T interpolation, AET=average absolute percentage error in T interpolation, MEK=maximum absolute percentage error in κ interpolation, and AEK=average absolute percentage error in κ interpolation.

Transition	Upsilon				Downsilon			
	MET	AET	MEK	AEK	MET	AET	MEK	AEK
1-2	0.069	0.012	0.562	0.021	0.012	0.002	0.367	0.024
1-3	0.178	0.025	0.562	0.024	0.017	0.001	0.308	0.020
1-4	0.464	0.074	0.563	0.072	0.017	0.002	0.319	0.021
1-5	0.586	0.088	0.872	0.093	0.014	0.002	0.313	0.021
2-3	0.112	0.018	0.562	0.022	0.017	0.001	0.312	0.021
2-4	0.461	0.074	0.563	0.072	0.017	0.002	0.319	0.021
2-5	0.584	0.088	0.868	0.093	0.014	0.002	0.313	0.021
3-4	0.459	0.074	0.563	0.071	0.017	0.002	0.319	0.021
3-5	0.581	0.088	0.860	0.093	0.014	0.002	0.313	0.021
4-5	0.455	0.078	0.571	0.075	0.017	0.005	0.304	0.020

Table 3. Sample \log_{10} of scaled Upsilon data for the 1-5 transition.

T	2.000	2.025	2.050	2.075	2.100	2.125	2.150	2.175	2.200	2.225	2.250	2.275	2.300
κ													
1.600	-7.085	-7.045	-7.005	-6.965	-6.925	-6.885	-6.845	-6.805	-6.765	-6.725	-6.685	-6.645	-6.605
1.625	-7.063	-7.022	-6.981	-6.941	-6.900	-6.860	-6.819	-6.778	-6.738	-6.697	-6.657	-6.616	-6.575
1.650	-7.056	-7.015	-6.974	-6.933	-6.892	-6.850	-6.809	-6.768	-6.727	-6.685	-6.644	-6.603	-6.562
1.675	-7.061	-7.019	-6.977	-6.935	-6.894	-6.852	-6.810	-6.768	-6.726	-6.684	-6.642	-6.601	-6.559
1.700	-7.073	-7.031	-6.988	-6.946	-6.903	-6.861	-6.818	-6.776	-6.733	-6.691	-6.648	-6.606	-6.563
1.725	-7.091	-7.048	-7.005	-6.961	-6.918	-6.875	-6.832	-6.789	-6.746	-6.703	-6.660	-6.617	-6.574
1.750	-7.113	-7.069	-7.025	-6.982	-6.938	-6.894	-6.850	-6.807	-6.763	-6.719	-6.676	-6.632	-6.588
1.775	-7.138	-7.094	-7.050	-7.005	-6.961	-6.917	-6.872	-6.828	-6.784	-6.739	-6.695	-6.651	-6.606
1.800	-7.167	-7.122	-7.077	-7.032	-6.987	-6.942	-6.897	-6.852	-6.807	-6.762	-6.717	-6.672	-6.627
1.825	-7.197	-7.152	-7.106	-7.061	-7.015	-6.969	-6.924	-6.878	-6.833	-6.787	-6.741	-6.696	-6.650
1.850	-7.230	-7.184	-7.137	-7.091	-7.045	-6.999	-6.953	-6.906	-6.860	-6.814	-6.768	-6.722	-6.675
1.875	-7.264	-7.217	-7.170	-7.124	-7.077	-7.030	-6.983	-6.936	-6.889	-6.843	-6.796	-6.749	-6.702
1.900	-7.300	-7.252	-7.205	-7.157	-7.110	-7.062	-7.015	-6.967	-6.920	-6.872	-6.825	-6.778	-6.730
1.925	-7.336	-7.288	-7.240	-7.192	-7.144	-7.096	-7.048	-7.000	-6.952	-6.904	-6.855	-6.807	-6.759
1.950	-7.374	-7.325	-7.277	-7.228	-7.179	-7.130	-7.082	-7.033	-6.984	-6.936	-6.887	-6.838	-6.790
1.975	-7.412	-7.363	-7.314	-7.264	-7.215	-7.166	-7.117	-7.067	-7.018	-6.969	-6.919	-6.870	-6.821
2.000	-7.452	-7.402	-7.352	-7.302	-7.252	-7.202	-7.152	-7.102	-7.052	-7.002	-6.952	-6.902	-6.853

Table 4. Sample \log_{10} of Downsilon data for the 1-5 transition.

T	2.000	2.025	2.050	2.075	2.100	2.125	2.150	2.175	2.200	2.225	2.250	2.275	2.300
κ													
1.600	-1.123	-1.117	-1.111	-1.105	-1.100	-1.096	-1.091	-1.088	-1.084	-1.081	-1.078	-1.075	-1.073
1.625	-1.145	-1.140	-1.135	-1.131	-1.128	-1.124	-1.121	-1.119	-1.116	-1.114	-1.112	-1.110	-1.108
1.650	-1.166	-1.162	-1.158	-1.155	-1.153	-1.150	-1.148	-1.146	-1.144	-1.142	-1.141	-1.139	-1.138
1.675	-1.185	-1.182	-1.179	-1.177	-1.175	-1.173	-1.171	-1.169	-1.168	-1.167	-1.165	-1.164	-1.163
1.700	-1.203	-1.200	-1.198	-1.196	-1.194	-1.193	-1.191	-1.190	-1.189	-1.188	-1.187	-1.186	-1.185
1.725	-1.219	-1.217	-1.215	-1.213	-1.212	-1.210	-1.209	-1.208	-1.207	-1.206	-1.206	-1.205	-1.204
1.750	-1.233	-1.231	-1.230	-1.228	-1.227	-1.226	-1.225	-1.224	-1.224	-1.223	-1.222	-1.222	-1.221
1.775	-1.246	-1.245	-1.244	-1.242	-1.241	-1.240	-1.240	-1.239	-1.238	-1.238	-1.237	-1.237	-1.236
1.800	-1.258	-1.257	-1.256	-1.255	-1.254	-1.253	-1.252	-1.252	-1.251	-1.251	-1.250	-1.250	-1.250
1.825	-1.269	-1.268	-1.267	-1.266	-1.266	-1.265	-1.264	-1.264	-1.263	-1.263	-1.262	-1.262	-1.262
1.850	-1.279	-1.278	-1.278	-1.277	-1.276	-1.275	-1.275	-1.274	-1.274	-1.274	-1.273	-1.273	-1.273
1.875	-1.289	-1.288	-1.287	-1.286	-1.286	-1.285	-1.285	-1.284	-1.284	-1.284	-1.283	-1.283	-1.283
1.900	-1.297	-1.297	-1.296	-1.295	-1.295	-1.294	-1.294	-1.293	-1.293	-1.293	-1.292	-1.292	-1.292
1.925	-1.305	-1.305	-1.304	-1.303	-1.303	-1.302	-1.302	-1.302	-1.301	-1.301	-1.301	-1.301	-1.301
1.950	-1.313	-1.312	-1.312	-1.311	-1.311	-1.310	-1.310	-1.309	-1.309	-1.309	-1.309	-1.309	-1.308
1.975	-1.320	-1.319	-1.319	-1.318	-1.318	-1.317	-1.317	-1.317	-1.316	-1.316	-1.316	-1.316	-1.316
2.000	-1.326	-1.326	-1.325	-1.325	-1.324	-1.324	-1.324	-1.323	-1.323	-1.323	-1.323	-1.323	-1.322